

## MATERIALS SCIENCE

# Exceptional plasticity in the bulk single-crystalline van der Waals semiconductor InSe

Tian-Ran Wei<sup>1,2\*</sup>, Min Jin<sup>3\*</sup>, Yuecun Wang<sup>4\*</sup>, Hongyi Chen<sup>2</sup>, Zhiqiang Gao<sup>2</sup>, Kumpeng Zhao<sup>1,2</sup>, Pengfei Qiu<sup>2</sup>, Zhiwei Shan<sup>4</sup>, Jun Jiang<sup>5</sup>, Rongbin Li<sup>3</sup>, Lidong Chen<sup>2†</sup>, Jian He<sup>6†</sup>, Xun Shi<sup>1,2†</sup>

Inorganic semiconductors are vital for a number of critical applications but are almost universally brittle. Here, we report the superplastic deformability of indium selenide (InSe). Bulk single-crystalline InSe can be compressed by orders of magnitude and morphed into a Möbius strip or a simple origami at room temperature. The exceptional plasticity of this two-dimensional van der Waals inorganic semiconductor is attributed to the interlayer gliding and cross-layer dislocation slip that are mediated by the long-range In-Se Coulomb interaction across the van der Waals gap and soft intralayer In-Se bonding. We propose a combinatory deformability indicator ( $\Xi$ ) to prescreen candidate bulk semiconductors for use in next-generation deformable or flexible electronics.

Inorganic semiconductors are versatile and have applications in information, sensor, catalysis, and energy technologies (1). Most bulk inorganic semiconductors are intrinsically brittle at ambient condition (2). The lack of intrinsic plasticity and deformability restricts the scope of application for bulk inorganic semiconductors. While doping or alloying may alter the electrical, magnetic, optical, and thermal properties of an inorganic semiconductor by orders of magnitude, doping hardly bestows any plasticity and deformability. A handful of examples, however, suggest that this is not always the case. Bulk single-crystalline ZnS is brittle under normal lighting but becomes plastically deformable in complete darkness at ambient temperature, as plastic deformation is inhibited by the trapping of photoexcited charge carriers and the electrostatic interactions between dislocation cores (3). Brittle materials in the bulk form can also exhibit plasticity as nanowires (4). The discovery of intrinsic plastic deformability in bulk Ag<sub>2</sub>S (5) has enabled the fabrication of a fully inorganic Ag<sub>2</sub>S-based flexible thermoelectric power generation module (6). The plasticity of bulk Ag<sub>2</sub>S is attributed to multicentered chemical bonding

and solid linkage among easy slip planes (5) or to easy motion of Ag-S octagons without breaking Ag-S bonds in the presence of metallic Ag-Ag bonding (7).

Aside from Ag<sub>2</sub>S, evidence for a wide range of bulk inorganic semiconductors being plastically deformable at ambient condition is not yet available. Note that two-dimensional van der Waals (2D vdW) inorganic materials gain pliability upon exfoliation, after thinning down to a monolayer or a few layers (8, 9). This observation follows the general rule that the bending modulus is proportional to the cube of the thickness (10), and thus the stiffness of a bulk material can be lowered by reducing its cross-sectional area (11–13). Hence, monolayer or few-layer 2D vdW inorganic semiconductors become promising candidates for nano-electronics (14, 15).

Still, plastic deformability is not expected for a bulk 2D vdW inorganic semiconductor at room temperature. The thickness-induced flexibility does not change the brittle nature of the material, and large stress during deformation can still rupture a material of finite thickness, especially for those high-elastic modulus materials such as graphene or graphite (16). In a typical 2D vdW bulk inorganic semiconductor, the intralayer bonding is often covalent or ionic-covalent, creating intralayer rigidity. The presence of a vdW gap makes the material easy to cleave, thus making it difficult for the material to retain its structural integrity through plastic deformation.

In this work, we discovered that indium selenide (InSe), a 2D vdW group IIIA metal chalcogenide, exhibits exceptional plasticity in the bulk single-crystalline form but not in the bulk polycrystalline form. We characterized and pinpointed the atomic origin of deformability and plasticity and proposed a deformability factor ( $\Xi$ ) to prescreen materials that can be morphed into various shapes for specific applications.

Despite the potential applications in electronics and optoelectronics (17–19), InSe is underutilized compared with other III-V and II-VI semiconductors. InSe adopts a layered structure in which each layer is formed by the In-Se honeycomb lattice in the *ab* plane, and the sequence of atoms in the *c* direction is Se-In-In-Se, with a vdW gap between Se and Se (Fig. 1A). These layers are stacked along the *c* axis with a period of  $\sim 0.8$  nm (*c*/2, where *c* is the lattice constant along the *c* axis). Different layer-stacking sequences lead to various polytypes (20–22). The as-grown InSe crystalline ingot (23) and its cleaved facets have a metallic luster (Fig. 1, B and C). The measurements of packing density, x-ray diffraction (XRD), and transmission electron microscope–selected-area electron diffraction (TEM-SAED) (fig. S1) corroborate that the InSe samples studied here are  $\beta$ -phase single crystals with a space group of  $P6_3/mmc$  (20). The unit cell contains two Se-In-In-Se layers, with the In atoms in one layer vertically aligned with Se atoms in the adjacent layer (Fig. 1A).

The as-grown InSe single crystal is a non-degenerate, native n-type semiconductor with a measured bandgap around 1.2 eV (fig. S2), consistent with previous reports (18, 24). The sheets peeled off from an InSe single crystal can be bent, wound, twisted into a Möbius strip, or folded into a simple origami (Fig. 1, D to F). Large deformation induces large local stress, as reflected by the few wrinkles and microcleavages on the compression side of an  $\sim 300$ - $\mu\text{m}$ -thick sheet ( $\sim 10^5$  unit cells along the *c* axis) that is folded into a “U” shape with an  $\sim 400$ - $\mu\text{m}$  radius semicircle without visible fractures (Fig. 1G). Rather than extending through the sample, these microcleavages and wrinkles are local, and most can be healed by gentle pressing after unfolding (fig. S3). Cyclic bending deformation is found to have a trivial effect on the photoluminescence and Raman spectra and a limited effect on the electrical resistance (fig. S4). Such exceptional deformability and plasticity are not observed in other 2D materials with similar thickness or in inorganic semiconductors such as SnSe and Bi<sub>2</sub>Te<sub>3</sub> (fig. S5). In fact, 2D materials such as graphene can only be folded and unfolded when they are one or a few layers thick (25) or by artificial microstructural manipulations (26).

As shown in Fig. 1, H and I, InSe crystals exhibit  $\sim 80\%$  compression strain along and perpendicular to the *c* axis. Because of the equipment limit, the ultimate strain is not reached. The serrations in the stress-strain curve indicate the dislocation nucleation, cross-link, and break off. Large plastic deformability is also confirmed in the uniaxial tensile tests (fig. S6A) and three-point bending tests (fig. S6B). Progressive roller pressing can compress a 660- $\mu\text{m}$ -thick crystal slab to the equipment limit of  $\sim 15$ - $\mu\text{m}$  thickness (fig. S7), corresponding

<sup>1</sup>State Key Laboratory of Metal Matrix Composites, School of Materials Science and Engineering, Shanghai Jiao Tong University, Shanghai 200240, China. <sup>2</sup>State Key Laboratory of High Performance Ceramics and Superfine Microstructure, Shanghai Institute of Ceramics, Chinese Academy of Sciences, Shanghai 200050, China. <sup>3</sup>College of Materials, Shanghai Dianji University, Shanghai 201306, China. <sup>4</sup>Center for Advancing Materials Performance from the Nanoscale (CAMP-Nano) and Hysitron Applied Research Center in China (HARCC), State Key Laboratory for Mechanical Behavior of Materials, Xi'an Jiaotong University, Xi'an 710049, China. <sup>5</sup>Ningbo Institute of Materials Technology and Engineering, Chinese Academy of Sciences, Ningbo 315201, China. <sup>6</sup>Department of Physics and Astronomy, Clemson University, Clemson, SC 29634-0978, USA.

\*These authors contributed equally to this work.

†Corresponding author. Email: cld@mail.sic.ac.cn (L.C.); jianhe@g.clemson.edu (J.H.); xshi@sjtu.edu.cn and xshi@mail.sic.ac.cn (X.S.)

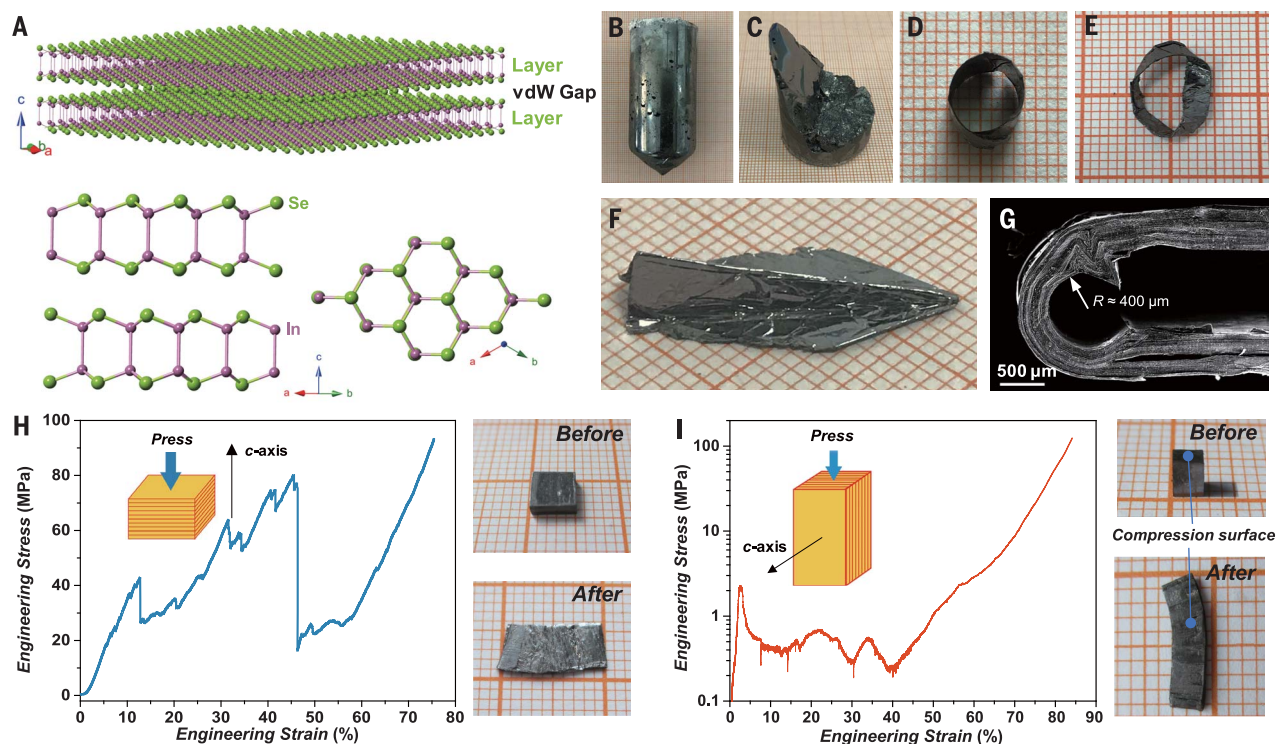


**Fig. 1. Deformability of InSe single crystals.** (A) Crystal structure of  $\beta$ -InSe and the projection on the (110) and (001) planes. (B) As-grown crystal and (C) cleavage surface. (D to F) InSe single crystal is morphed into various shapes without breaking. (G) Scanning electron microscopy (SEM) image of a folded crystal slab.  $R$ , radius. Compression engineering stress-strain curves along (H) and perpendicular to (I) the  $c$  axis. The smallest grid denotes 1 mm in all photographs.

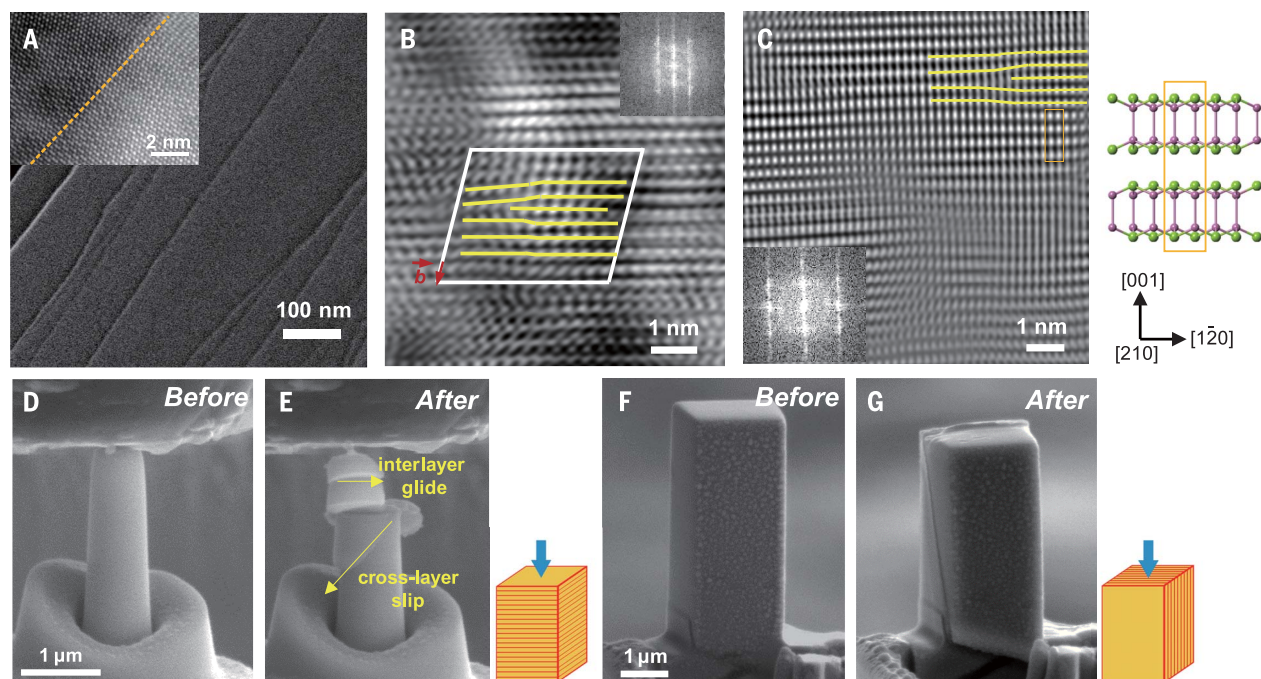


**Fig. 2. Microscopic characterization and in situ SEM compression tests revealing the plasticity mechanisms of InSe.** (A to C) TEM-STEM analyses of deformed InSe crystal: the zone axis is along (A) and perpendicular to [(B) and (C)] the  $c$  axis. (A) The slip steps are the result of easy interlayer gliding. The inset is the inverse Fourier transform from dark-field STEM (IFT-DF-STEM) image of the area near the slip step (dashed orange line). [(B) and (C)] IFT-DF-STEM images of edge dislocations. Yellow lines highlight the edge dislocation. (D to G) In situ SEM compression tests on InSe micropillars along [(D) and (E)] and perpendicular to [(F) and (G)] the  $c$  axis, showing interlayer gliding and cross-layer slip.

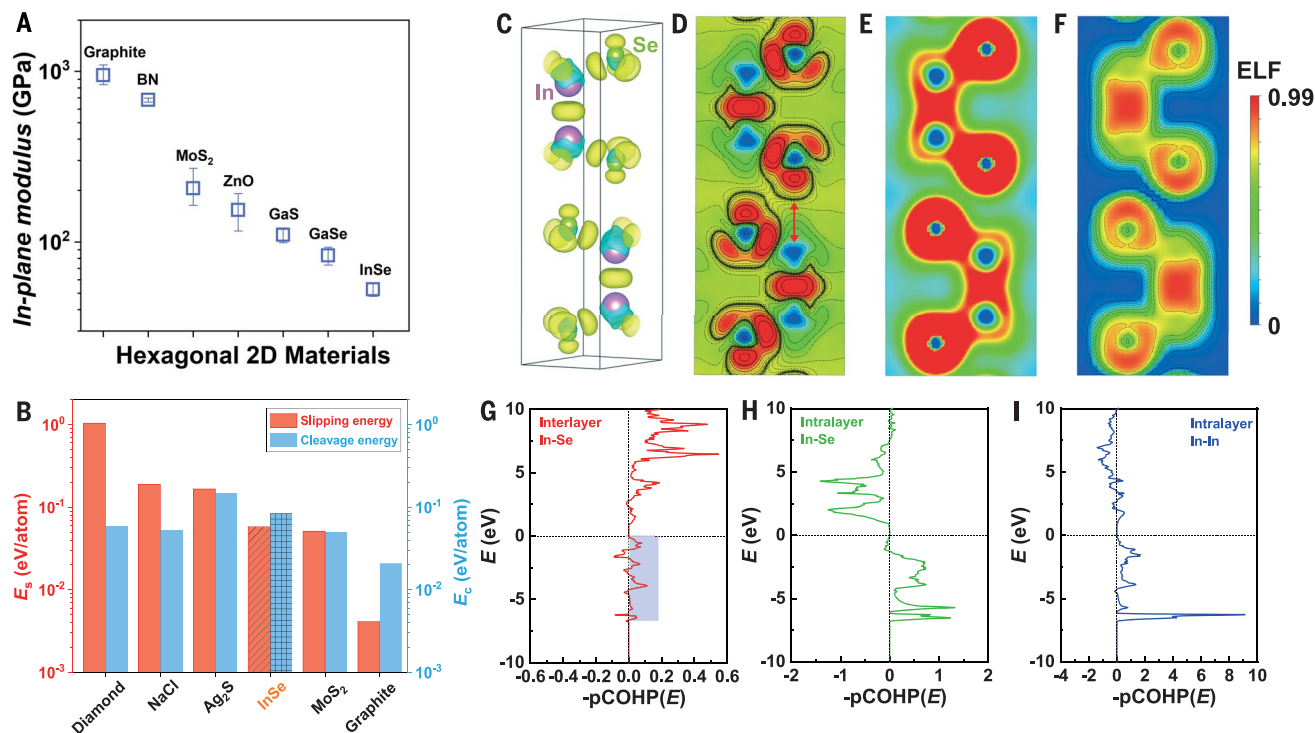


**Fig. 3. Bond characters of InSe.** (A) Intralayer modulus of InSe and several other hexagonal 2D inorganic semiconductors (table S1). (B) Calculated slipping energy ( $E_s$ , red, left axis) and cleavage energy ( $E_c$ , blue, right axis) for several representative

materials. (C) Differential charge density and (D) projection on the (110) plane. (E) Charge density. (F) Electron localization function (ELF). (G to I) COHPs for interlayer In-Se bonding (G), intralayer In-Se bonding (H), and intralayer In-In bonding (I).

to a total compression ratio of >4000%. Brittle materials are shattered through a similar compression process. Scanning transmission electron microscopy (STEM) and TEM characterization of the deformed InSe single crystal provide atomic-scale details of plastic deformation and hints of the underlying mechanism. As shown in Fig. 2A and fig. S1, the intralayer lattice is nearly perfect, with very few defects; the slip steps are the sign of interlayer gliding. Meanwhile, the cross-layer lattice contains abundant defects, such as stacking faults, consistent with the streaked SAED spots (fig. S8A). Figure S8B displays the continuous, smooth, and fracture-free bending over many layers in a collective fashion that underlies the macroscopic bendability. Edge dislocations are clearly seen in Fig. 2, B and C, with the extra half-plane of atoms parallel to the basal  $ab$  plane. The cross-layer dislocation slip thus enables shear deformation under compression.

We also conducted in situ SEM uniaxial compression tests on the InSe single-crystalline micropillars along and perpendicular to the  $c$  axis (Fig. 2, D to G, and fig. S9). Consistent with the results of macroscopic compression tests (Fig. 1, H and I), the stress-strain curve of microscopic compression tests clearly shows slip-induced strain bursts (fig. S9), similar to those of metals (27), and the morphology after

testing is free of discernible cleavage, confirming the exceptional plasticity. Through the process of compression, interlayer gliding occurs first, followed by cross-layer dislocation slip, as evidenced by the cross-layer shear band [Fig. 2, D to G, and movies S1 and S2 (23)]. The shear band angle (Fig. 2E) and the XRD patterns of roller-pressed samples (fig. S10) suggest the (10L) slip planes. Hence, it is the interlayer gliding and the cross-layer dislocation slip that enable the exceptional plasticity of bulk InSe single crystal.

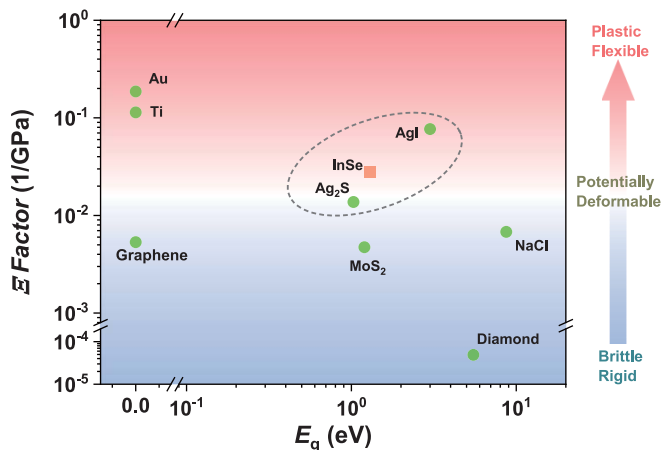
To elucidate the atomic origin of the exceptional plasticity of bulk InSe single crystal, we inspected the intra- and interlayer interactions. For intralayer mechanical properties, we used the elastic stiffness constants ( $c_{ij}$ ) data to deduce the intralayer Young's modulus  $E_{in}$ , which is isotropic within the  $ab$  plane of a hexagonal crystal lattice (23). The  $E_{in}$  value essentially reflects the intralayer bond rigidity, and the contribution from interlayer interactions is small. The  $E_{in}$  of InSe is  $\sim 53$  GPa (Fig. 3A), among the lowest for the hexagonal-structured semiconductors, and explains the pliability of mono- or few-layer InSe.

Given the difficulty of experimentally characterizing the interlayer interactions and relative glide process, we invoked density functional theory calculations. On the basis of our TEM

observations, we assume that the (001) planes slip along the [100] direction in InSe. For convenience, we divide each slipping period into 12 steps and calculate the energy variation versus the interplanar distance for each step (23). The slipping energy ( $E_s$ ) barrier of InSe is as low as 0.058 eV per atom (Fig. 3B). In contrast, the cleavage energy ( $E_c$ ) is 0.084 eV per atom, which is much higher than that of 2D MoS<sub>2</sub> and graphene. The  $E_c$  of InSe is also substantially higher than that of well-known brittle materials such as NaCl and diamond. The small slipping energy  $E_s$  points toward an easy interlayer gliding, while the relatively large cleavage energy  $E_c$  value favors a strong interlayer integrity during slip. Facilitated by the interlayer gliding and cross-layer slip (compare Fig. 2, D to G), plastic deformation takes place. The interlayer interaction, along with the pliable layers, makes large plastic deformation possible. The plasticity of InSe is strongly anisotropic owing to the limited slip systems.

The intralayer and interlayer interactions have a common origin in chemical bonding. We calculated the charge density map and the differential charge density map. One Se atom is bonded with three In atoms in one layer, leaving lone-pair electron lobes pointing to the interlayer van der Waals gap (Fig. 3, C and D). The electron localization function (ELF) of the

**Fig. 4. Deformability factor  $\Xi = (E_c/E_s)(1/E_{in})$  as a function of bandgap ( $E_g$ ).**  $E_c$  and  $E_s$  are the cleavage energy and slipping energy of the slip system, respectively;  $E_{in}$  is the Young's modulus along the slip direction.



intralayer In-Se bond is as low as 0.34 to 0.5 (Fig. 3F), which is comparable to that of metals (28), suggesting a considerable degree of delocalization, a low bond rigidity, and thus a low intralayer modulus (Fig. 3A). Similarly, one In atom is bonded to three Se atoms and another In atom. The In-In bond in the slab has a high ELF of 0.94 and a strong, sharp peak in the crystal orbital Hamilton population (COHP) (Fig. 3I), indicating a localized covalent feature.

For the interlayer interactions, we clearly see the Se-Se interaction from the distortion of the electron cloud in the differential charge density maps (Fig. 3, C and D). The vdW-like force is the prevalent feature of 2D materials. Of special interest is the presence of a long-range Coulombic interaction reflected in the charge density distortion between In and Se atoms across the layer (Fig. 3D, red arrows), spreading from 0 to  $-7$  eV in the calculated COHP (Fig. 3G, blue rectangle). This long-range Coulombic In-Se interlayer interaction explains the peak-splitting in the Raman and infrared spectra of InSe (29) and GaSe (30). Here, the long-range coulombic In-Se interlayer interaction and the Se-Se vdW-like force work in tandem with a sufficiently large  $E_c$  to enable the interlayer gliding and cross-layer dislocation slip while retaining the structural integrity through plastic deformation.

More important than the specific criteria for deformability in InSe and  $Ag_2S$  is the development of a more general rule to find other candidate bulk materials. Any criteria should apply to both  $Ag_2S$  and InSe. As the deformability and bendability of 2D materials require large cleavage energy ( $E_c$ ) and small slipping energy ( $E_s$ ) to facilitate plastic deformation as well as pliable layers with low modulus to allow elastic bending, we propose that a deformability factor  $\Xi = (E_c/E_s)(1/E_{in})$  (in units of inverse gigapascals) might be useful to prescreen bendable and deformable inorganic semiconductors. The  $E_c/E_s$  ratio quantifies the plasticity of the material that is in line with the criterion

proposed by Rice *et al.* (31, 32), while  $E_{in}$  is the in-plane Young's modulus along the slip direction. We summarize  $\Xi$  as a function of the bandgap ( $E_g$ ) for a number of representative materials (Fig. 4). Metals are in the top-left corner with extremely large plasticity and deformability but zero bandgap. The wide-bandgap inorganic materials such as NaCl and diamond are in the bottom-right corner with brittleness and sizable bandgap. Notably, deformable semiconductor  $Ag_2S$  and InSe have close  $\Xi$  values, and they are located in the middle area with medium bandgaps. The diagram also shows that  $\beta$ -AgI with a large bandgap ( $\sim 2.9$  eV) should be deformable. This seems to be the case according to early literature (33). The  $\Xi$ - $E_g$  diagram can thus be used as a guide to prescreen and develop deformable and plastic bulk inorganic semiconductors, especially in the vicinity of InSe and  $Ag_2S$ .

In this work, we discovered exceptional deformability and plasticity in bulk single-crystalline InSe, the first of its kind in van der Waals inorganic semiconductors. We envisage applications in deformable and flexible thermoelectric devices, sensors, and photodetectors, to name a few. The results of comprehensive experimental and theoretical study corroborate that such extraordinary mechanical properties stem from both the intralayer pliability and the interlayer long-range In-Se coulombic interaction across the van der Waals gap, a trade-off and synergy between the retention of substructures and multiple easy slip pathways. We believe that our proposed deformability factor will help guide materials development for discovering other bulk semiconductors useful in next-generation deformable or flexible electronics.

#### REFERENCES AND NOTES

1. K. Seeger, *Semiconductor Physics: An Introduction* (Springer, ed. 9, 2004).
2. K. T. Faber, K. J. Malloy, *The Mechanical Properties of Semiconductors*, vol. 37 of *Semiconductors and Semimetals* (Academic Press, 1992).

3. Y. Oshima, A. Nakamura, K. Matsunaga, *Science* **360**, 772–774 (2018).
4. X. D. Han *et al.*, *Adv. Mater.* **19**, 2112–2118 (2007).
5. X. Shi *et al.*, *Nat. Mater.* **17**, 421–426 (2018).
6. J. Liang *et al.*, *Energy Environ. Sci.* **12**, 2983–2990 (2019).
7. G. Li *et al.*, *npj Comput. Mater.* **4**, 44 (2018).
8. S. Das, J. A. Robinson, M. Dubey, H. Terrones, M. Terrones, *Annu. Rev. Mater. Res.* **45**, 1–27 (2015).
9. S. J. Kim, K. Choi, B. Lee, Y. Kim, B. H. Hong, *Annu. Rev. Mater. Res.* **45**, 63–84 (2015).
10. S. P. Timoshenko, S. Woinowsky-Krieger, *Theory of Plates and Shells* (McGraw-Hill, ed. 2, 1959).
11. J. A. Rogers, T. Someya, Y. Huang, *Science* **327**, 1603–1607 (2010).
12. H. Li, Z. Tang, Z. Liu, C. Zhi, *Joule* **3**, 613–619 (2019).
13. J. Peng, G. J. Snyder, *Science* **366**, 690–691 (2019).
14. G. R. Bhimanapati *et al.*, *ACS Nano* **9**, 11509–11539 (2015).
15. G. Fiori *et al.*, *Nat. Nanotechnol.* **9**, 768–779 (2014).
16. C. Lee, X. Wei, J. W. Kysar, J. Hone, *Science* **321**, 385–388 (2008).
17. T. Shen, J.-C. Ren, X. Liu, S. Li, W. Liu, *J. Am. Chem. Soc.* **141**, 3110–3115 (2019).
18. D. A. Bandurin *et al.*, *Nat. Nanotechnol.* **12**, 223–227 (2017).
19. S. R. Tamalampudi *et al.*, *Nano Lett.* **14**, 2800–2806 (2014).
20. S. Popović, A. Tonejc, B. Gržeta-Plenković, B. Čelustka, R. Trojko, *J. Appl. Cryst.* **12**, 416–420 (1979).
21. J. Rigault, A. Rimsky, A. Kuhn, *Acta Crystallogr. B* **36**, 916–918 (1980).
22. G. Han, Z. G. Chen, J. Drennan, J. Zou, *Small* **10**, 2747–2765 (2014).
23. Materials and methods are available as supplementary materials.
24. S. Lei *et al.*, *ACS Nano* **8**, 1263–1272 (2014).
25. H. Chen *et al.*, *Science* **365**, 1036–1040 (2019).
26. L. Peng *et al.*, *Adv. Mater.* **29**, 1700589 (2017).
27. Z.-J. Wang *et al.*, *Appl. Phys. Lett.* **100**, 071906 (2012).
28. A. Ormezi, H. Rosner, F. R. Wagner, M. Kohout, Y. Grin, *J. Phys. Chem. A* **110**, 1100–1105 (2006).
29. C. Carlone, S. Jandl, H. R. Shanks, *Phys. Status Solidi B* **103**, 123–130 (1981).
30. T. Wieting, J. Verble, *Phys. Rev. B* **5**, 1473–1479 (1972).
31. J. R. Rice, *J. Mech. Phys. Solids* **40**, 239–271 (1992).
32. J. R. Rice, R. Thomson, *Philos. Mag.* **29**, 73–97 (1974).
33. S.-I. Pyun, J.-S. Bae, *J. Power Sources* **63**, 109–113 (1996).

#### ACKNOWLEDGMENTS

We thank F. Xu and C. Zhu at the Shanghai Institute of Ceramics, Chinese Academy of Sciences, for assisting with the TEM-STEM experiments and analyses, and C. Guo at Xi'an Jiaotong University for assistance with the micropillar compression tests.

**Funding:** This work is supported by the National Key Research and Development Program of China (2018YFB0703600 and 2017YFB0702001), the National Natural Science Foundation of China (51625205, 91963208, 51961135106, and 51902249), and the Nature Science Foundation of Shanghai (19ZR1419900). M.J. and R.L. acknowledge the support of the Shanghai Engineering Research Center of Hot Manufacturing (18DZ2253400). **Author contributions:** T.-R.W., M.J., J.J., and R.L. prepared the samples and measured the physical properties. T.-R.W. and Z.G. measured the mechanical properties. H.C. performed ab initio calculations. Y.W. and Z.S. performed in situ SEM mechanical tests. T.-R.W., Y.W., H.C., Z.G., K.Z., and P.Q. collected the data and provided explanation and model under the guidance of X.S., J.H., and L.C. T.-R.W., M.J., Y.W., L.C., J.H., and X.S. wrote and edited the manuscript. All authors contributed helpful discussions to this work. **Competing interests:** The authors declare no competing interests. **Data and materials availability:** All data are available in the manuscript and the supplementary materials.

#### SUPPLEMENTARY MATERIALS

science.sciencemag.org/content/369/6503/542/suppl/DC1  
Materials and Methods  
Supplementary Text  
Figs. S1 to S11  
Tables S1 and S2  
References (34–52)  
Movies S1 and S2

21 January 2020; accepted 8 June 2020  
10.1126/science.aba9778

## Exceptional plasticity in the bulk single-crystalline van der Waals semiconductor InSe

Tian-Ran Wei, Min Jin, Yuecun Wang, Hongyi Chen, Zhiqiang Gao, Kunpeng Zhao, Pengfei Qiu, Zhiwei Shan, Jun Jiang, Rongbin Li, Lidong Chen, Jian He and Xun Shi

*Science* **369** (6503), 542-545.  
DOI: 10.1126/science.aba9778

### Deformable semiconductors

Semiconductors are usually brittle and do not deform easily. Wei *et al.* found that bulk single crystals of indium selenide instead have excellent flexibility (see the Perspective by Han). The deformability comes from the compliant intralayer bonding between indium and selenium. The authors used these observations along with a previously discovered silver sulfide to determine a deformability factor for materials that may help find other deformable semiconductors.

*Science*, this issue p. 542; see also p. 509

#### ARTICLE TOOLS

<http://science.sciencemag.org/content/369/6503/542>

#### SUPPLEMENTARY MATERIALS

<http://science.sciencemag.org/content/suppl/2020/07/29/369.6503.542.DC1>

#### RELATED CONTENT

<http://science.sciencemag.org/content/sci/369/6503/509.full>

#### REFERENCES

This article cites 48 articles, 5 of which you can access for free  
<http://science.sciencemag.org/content/369/6503/542#BIBL>

#### PERMISSIONS

<http://www.sciencemag.org/help/reprints-and-permissions>

Use of this article is subject to the [Terms of Service](#)

---

*Science* (print ISSN 0036-8075; online ISSN 1095-9203) is published by the American Association for the Advancement of Science, 1200 New York Avenue NW, Washington, DC 20005. The title *Science* is a registered trademark of AAAS.

Copyright © 2020 The Authors, some rights reserved; exclusive licensee American Association for the Advancement of Science. No claim to original U.S. Government Works